Journal of Solid State Chemistry **160,** 39–44 (2001)
doi:10.1006/jssc.2000.9180, available online at http://www.idealibrary.com on IDEAL®

# Polarized X-Ray Absorption Spectroscopic Study on Mercuric Bromide Intercalated $Bi_2Sr_2CaCu_2O_y$ Single Crystal

Seong-Ju Hwang and Jin-Ho Choy[1]

*National Nanohybrid Materials Laboratory, School of Chemistry and Molecular Engineering, Seoul National University, Seoul 151-747, Korea*

Received October 23, 2000; in revised form March 7, 2001; accepted March 26, 2001; published online May 30, 2001

**Polarized X-ray absorption spectroscopic experiments have been carried out for the mercuric bromide intercalated $Bi_2Sr_2CaCu_2O_y$ single crystal, in order to understand the variation of anisotropic resistivities upon $HgBr_2$ intercalation as well as to probe the electronic structure of $HgBr_2$ intercalate. The Br K- and Bi $L_{III}$-edge spectra indicate a significant electron transfer from bismuth to bromine, implying an overlap between Bi 6*s* and Br 4*p* orbitals. From the Hg $L_{III}$- and Br K-edge data, it is also found that $HgBr_2$ intercalation gives rise to an electron localization in the (Hg–Br) bond, which leads to poor electronic conduction along the intercalant layer. In this context, the semiconducting out-of-plane resistivity of $HgBr_2$ intercalate can be explained by the poor conductivity of the intercalated $HgBr_2$ layer, even though the orbital overlap between Bi and Br facilitates the electron conduction between host and guest along the *c*-axis.** © 2001 Academic Press

## INTRODUCTION

The remarkable anisotropy in normal state properties is believed to be one of the most important features of high-$T_c$ superconductors, since it can provide insight for attaining a complete understanding of the high-$T_c$ superconducting phenomenon (1, 2). Among high-$T_c$ superconducting materials, the most severe anisotropy in transport properties was reported for the Bi-based cuprates in which the ratio of out-of-plane to in-plane resistivities can be of the order of $10^4$ (3, 4). In order to explain such a strong dependence of conductivity on the crystal direction, several models assuming interlayer tunneling or weak coupling have been proposed for *c*-axis conduction (4–7). Nevertheless, the validity of these theoretical models has remained controversial. In this regard, the application of intercalation to high-$T_c$ superconductors can provide useful information on the mechanism for *c*-axis conduction, since the intercalation allows us to control the interlayer distance along the *c*-axis. Previously, the anisotropic resistivities of iodine intercalate were measured in comparison with those of pristine $Bi_2Sr_2CaCu_2O_y$ (denoted hereafter as Bi2212). It was found that the iodine intercalation dramatically alters the semiconducting *c*-axis resistivity of the pristine compound to the metallic one, whereas it has little influence on the in-plane conduction (8, 9). Although theoretical models based on the interlayer coupling scheme cannot explain the variation of *c*-axis conduction upon iodine intercalation (8), the band calculation and X-ray absorption spectroscopic (XAS) results indicate that the chemical interaction between BiO layers becomes enhanced through the interaction between iodine and bismuth, leading to the metallization of *c*-axis resistivity (10, 11).

Recently we have developed new mercuric halide intercalated Bi2212 compounds, in which the superconducting Bi2212 blocks are alternatively interstratified with mercuric halide layers (12). According to the previous X-ray diffraction (XRD) and extended X-ray absorption fine structure (EXAFS) analyses, it was found that the linear mercuric halide molecule is stabilized in between BiO layers of Bi2212 blocks, as illustrated in Fig. 1 (13). On the other hand, the anisotropic resistivity measurements on the $HgBr_2$ intercalated Bi2212 single crystal revealed that the temperature dependence of the *c*-axis resistivity of Bi2212 remains nearly the same before and after $HgBr_2$ intercalation, which surely contrasts with the case of iodine intercalation (14). For the purpose of explaining such dissimilar effects of $HgBr_2$ and iodine intercalation, it is highly necessary to probe the electronic structure of $HgBr_2$ intercalated Bi2212, which is closely related to its conducting behavior (10). In this context, the polarized XAS experiment with various angles of incident X-ray radiation is expected to be quite effective for achieving understanding of the temperature dependence of the anisotropic conductivity of high-$T_c$ superconductors.

In this study, we have carried out polarized XAS experiments at Hg $L_{III}$-, Br K-, Cu K-, and Bi $L_{III}$-edges for the single crystalline Bi2212 and its $HgBr_2$ intercalate. The aim of this work is to probe the effect of $HgBr_2$ intercalation on the electronic structure along the *ab*-plane and *c*-axis.

[1] To whom correspondence should be addressed. Fax: + 82-2-872-9864. E-mail: jhchoy@plaza.snu.ac.kr.



0022-4596/01 $35.00

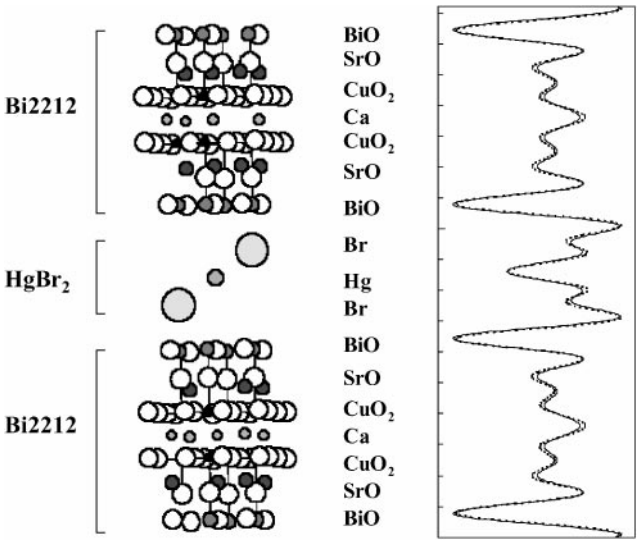


**FIG. 1.** Crystal structure of $(HgBr_2)_{0.5}Bi2212$, together with the one-dimensional electron density map along the *c*-axis. The dotted and solid lines represent the calculated electron density based on the intensities of the (00*l*) reflections in the XRD pattern and that on the basis of structural parameters calculated from the present crystal structure, respectively (13).

Especially, an attempt has been made to explain the variation of *c*-axis resistivity upon $HgBr_2$ intercalation on the basis of the present XAS results.

## EXPERIMENTAL

A single crystal of pristine Bi2212 was synthesized by the traveling-solvent floating-zone method, while the polycrystalline Bi2212 was prepared by conventional solid-state reaction. The intercalation of $HgBr_2$ was achieved by heating a vacuum-sealed Pyrex tube containing mercuric bromide and Bi2212 single crystal or polycrystal (mole ratio of 5:1) at 230°C in a uniform temperature furnace (12). The formation of single phasic intercalate was confirmed by the XRD pattern. According to least-square refinement, the *c*-axis unit-cell parameters were determined to be 30.6 Å for the pristine Bi2212 and 43.2 Å for its $HgBr_2$ intercalate. Since there are two intercalated layers of $HgBr_2$ for each unit cell of Bi2212, each mercuric bromide layer expands the *c*-axis by about 6.3 Å, as shown in Fig. 1 (12).

Thermogravimetric analysis (TGA) was carried out for the $HgBr_2$ intercalate using DuPont 2000 thermal analysis station in order to determine the amount of guest species introduced into host lattice. The total weight loss of the $HgBr_2$ intercalate in the temperature range of 20–500°C was determined to be 17.0%, which was in excellent agreement with the calculated value of $(HgBr_2)_{0.5}Bi_2Sr_2CaCu_2O_y$ (17.3%). The stoichiometry obtained from TGA was also confirmed by electron probe microanalysis (repeated five times), where the average atomic ratio among Hg, Br, and Bi was estimated to be 0.5:1:2 (15).

The X-ray absorption measurements were carried out at Photon Factory on beam line 10B using the silicon (311) channel-cut monochromator (16). The polarized spectra for single crystals were measured using fluorescence mode, whereas the unpolarized spectra for polycrystalline samples were collected with transmission mode. To obtain higher signals for the single crystals, the collages of similarly oriented small crystals were carefully assembled on adhesive tape. Two kinds of polarization angles between the *c*-axis and polarization vector **E**, $\theta = 10^\circ$ ($\mathbf{E}//c$) and $90^\circ$ ($\mathbf{E}\perp c$), were applied to obtain the polarized spectra. To ensure the reliability of the spectra, much care was taken to evaluate the stability of the energy scale by monitoring the spectra of Cu metal, $Bi_2O_3$, and $HgBr_2$ for each measurement. The inherent background in the data was removed by fitting a polynomial to the pre-edge region and extrapolating through the entire spectrum, from which it was subtracted. The resulting spectra, $\mu(E)$, were normalized to an edge jump of unity. In case of the Bi $L_{III}$-edge (13,426 eV), we have some difficulties in the normalization procedure due to the lack of a suitable extent of atomic-like post-edge data caused by the interference of the adjacent Br K-edge (13,470 eV). For this reason, the Bi $L_{III}$-edge XANES data of $HgBr_2$ intercalate were carefully normalized for comparing directly with those of pristine Bi2212. On the other hand, the nearly overlapping energies of Bi $L_{III}$- and Br K-edges might give rise to a considerable distortion to Br K-edge data by the preceding and underlying Bi $L_{III}$-edge signals. Such a spectral distortion is expected to be much more severe for the transmission data than for the fluorescence ones, since the former was vitiated by a significant background contribution from the Bi $L_{III}$-edge signals, whereas the possible distortion in the latter was mitigated by energy resolution of the Br K$\alpha$ fluorescent X-rays. In this context, we have tried to remove a distortion of the Br K-edge transmission spectrum of $HgBr_2$ intercalate by subtracting the Bi $L_{III}$-edge spectrum of $HgI_2$ intercalate from the distorted original spectra. Such a data correction can be reasonably accepted since both mercuric halide intercalates are expected to have a similar chemical environment of bismuth and, moreover, the Bi $L_{III}$-edge EXAFS signal in this region is much weaker compared to the Br K-edge XANES one (13). Actually, we could not observe any significant spectral changes in the Br K-edge transmission spectra of $HgBr_2$ intercalate before and after correction. In this regard, we could conclude that no correction is needed for the present data.

## RESULTS AND DISCUSSION

The polarized Hg $L_{III}$-edge XANES spectra of the $HgBr_2$ intercalated Bi2212 single crystal with polarization angles of

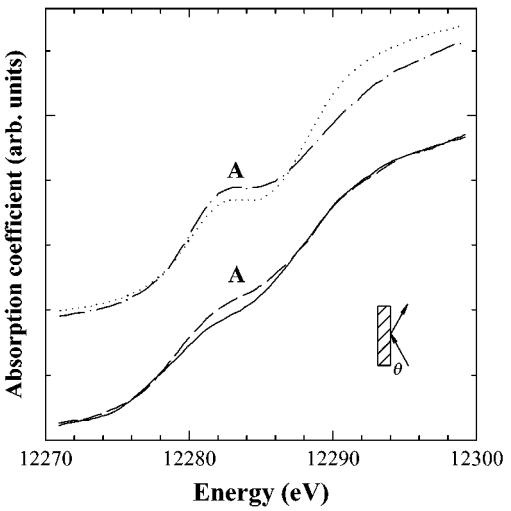


**FIG. 2.** Polarized Hg $L_{III}$-edge XANES spectra for $HgBr_2$ intercalated Bi2212 single crystal with polarization angles of 10° (**E**//$c$; solid lines) and 90° (**E**⊥$c$; dashed lines), in comparison with unpolarized spectra for free $HgBr_2$ (dotted lines) and $HgBr_2$ intercalated Bi2212 (dot-dashed lines). For the clear depiction of spectral features, the unpolarized spectra are shifted upward along the $y$-axis.

$\theta = 10°$ (**E**//$c$) and 90° (**E**⊥$c$) are presented in Fig. 2, together with the unpolarized spectra of free $HgBr_2$ and polycrystalline $HgBr_2$ intercalate. The selection rule for photoelectric excitation in the dipolar approximation predicts that the transitions to final states with orbital angular momentum quantum number $l_f$, which is different from the initial state with $l_i$ by $\pm 1$ unit, are allowed. Since all the present compounds possess $Hg^{+II}$ ions with vacant 6$s$ orbitals, the pre-edge peak A corresponding to $2p_{3/2} \rightarrow 6s$ is commonly observed for the reference $HgBr_2$ and the $HgBr_2$ intercalate (17). As shown in Fig. 2, the intensity of peak A is stronger for the polycrystalline $HgBr_2$ intercalate than for the free $HgBr_2$ (18), indicating that the chemical environment of mercury becomes more ionic upon $HgBr_2$ intercalation, together with an increase of hole density in the Hg 6$s$ orbital. Comparing the polarized spectra of $HgBr_2$ intercalate, the **E**⊥$c$ spectrum shows a stronger peak A with respect to the **E**//$c$ spectrum. Since the linear $HgBr_2$ molecule is significantly tilted with respect to the $c$-axis (65°), the spectrum with **E**⊥$c$ geometry provides information on the bonding character along the (Hg–Br) bond (13). In this respect, the higher intensity of peak A in the **E**⊥$c$ spectrum allows us to conclude that the increase of hole concentration in the Hg 6$s$ orbital can be attributed to the enhancement of ionic character in the (Hg–Br) bond, that is, an electron localization (19). Such an increase of ionicity of the (Hg–Br) bond can be understood on the basis of the competing bonding model, in which the significant interaction between Br and Bi induces the weakening of the competing (Hg–Br) bond with an enhancement of its ionic character. This is further evidenced by the previous micro-Raman study where the frequency of the symmetric stretching mode of (Hg–Br) bond, $\nu_1$(Hg–Br), is found to be smaller for the $HgBr_2$ intercalate than for the free $HgBr_2$ solid, implying the increase of ionicity of (Hg–Br) bond (20).

The polarized Br K-edge spectra with polarization angles of $\theta = 10°$ (**E**//$c$) and 90° (**E**⊥$c$) for the $HgBr_2$ intercalated Bi2212 single crystal are compared with the unpolarized spectra for reference $HgBr_2$ and polycrystalline $HgBr_2$ intercalate in Fig. 3. While the free $HgBr_2$ exhibits a strong pre-edge peak A corresponding to the transition from the core 1$s$ level to the unoccupied 4$p$ state, this peak is markedly depressed upon $HgBr_2$ intercalation. Since the intensity of this pre-edge peak is directly proportional to the density of the unoccupied Br 4$p$ final state, a remarkable decrease in the peak intensity upon intercalation demonstrates that the hole density in Br 4$p$ orbital is decreased upon intercalation. Judging from the fact that the peak depression appears to be stronger for the **E**⊥$c$ spectrum than for the **E**//$c$ one, such a partial filling of the unoccupied level of Br 4$p$ orbitals would originate mainly from the increase of ionicity of (Hg–Br) bond. In addition to the variation of peak intensity, there is a significant edge shift toward high energy in the **E**⊥$c$ spectrum compared to the **E**//$c$ one. This can be understood by the fact that the formation of the (Hg–Br) bond leads to a higher energy state of the Br $4p_\sigma^*$ antibonding orbital with respect to that of Br $4p_\pi^*$ (21).

Figure 4 represents the unpolarized and the polarized Cu K-edge XANES spectra for the pristine Bi2212 and its $HgBr_2$ intercalate, respectively. The polarized spectra exhibit remarkable spectral differences depending upon the polarization angles. From the polarization dependence of

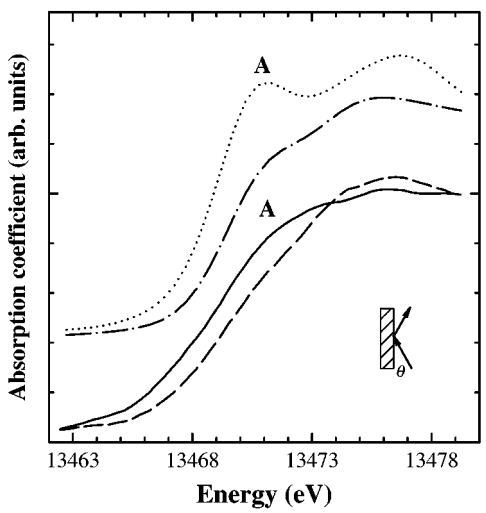


**FIG. 3.** Polarized Br K-edge XANES spectra for $HgBr_2$ intercalated Bi2212 single crystal with polarization angles of 10° (**E**//$c$; solid lines) and 90° (**E**⊥$c$; dashed lines), in comparison with unpolarized spectra for free $HgBr_2$ (dotted lines) and $HgBr_2$ intercalated Bi2212 (dot-dashed lines). For the clear depiction of spectral features, the unpolarized spectra are shifted upward along the $y$-axis.

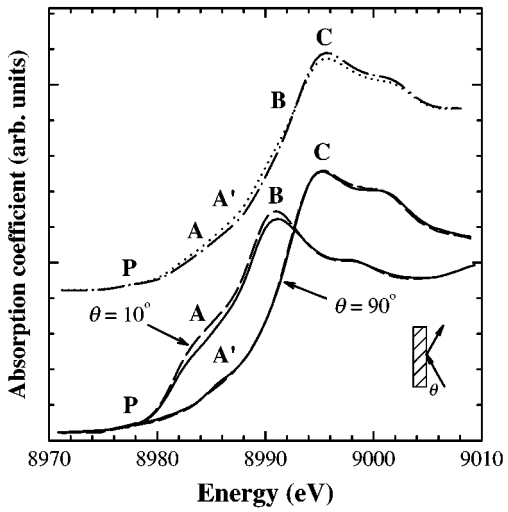


**FIG. 4.** Polarized Cu K-edge XANES spectra for the pristine Bi2212 single crystal (solid lines) and its $HgBr_2$ intercalate (dashed lines) with polarization angles of 10° (**E**//$c$) and 90° (**E**⊥$c$), in comparison with unpolarized spectra for Bi2212 (dotted lines) and $HgBr_2$ intercalate (dot-dashed lines). For the clear depiction of spectral features, the unpolarized spectra are shifted upward along the $y$-axis.

the spectral features, the peaks A and B are associated with the transitions from the 1$s$ orbital to the out-of-plane $4p_\pi$ orbital with and without shakedown process. In contrast, the features A′ and C are ascribed to in-plane $4p_\sigma$ orbital transitions with and without shakedown process, respectively (22). A small pre-edge peak P corresponding to the quadrupole-allowed $1s \rightarrow 3d$ transition is clearly detected for the **E**⊥$c$ spectra but almost concealed in the **E**//$c$ spectra. Such a phenomenon can be verified by considering the electronic configuration of divalent copper ion, [Ar] $(3d_{xy})^2(3d_{yz})^2(3d_{zx})^2(3d_z^2)^2(3d_{x-y}^2)^1$. That is, there is a hole in the $3d_{x-y}^2$ orbital which is available for the **E**⊥$c$ spectra, whereas the $3d_z^2$ orbital corresponding to the **E**//$c$ spectra is fully occupied by electrons. Upon $HgBr_2$ intercalation, no significant change in the position of spectral features is usually observed for either the unpolarized or the polarized spectra, suggesting that the effect of intercalation on the oxidation state of $CuO_2$ layer is too small to be detected by Cu K-edge XANES spectroscopy. Considering a minute $T_c$ decrease upon $HgBr_2$ intercalation which is even smaller than that upon iodine intercalation (12), an insignificant edge shift is thought to be quite reasonable because the edge shift induced by iodine intercalation was found to be only 0.1 eV (11). However, the slight oxidation of the $CuO_2$ layer upon $HgBr_2$ intercalation was already demonstrated by previous Cu K-edge EXAFS analyses, revealing that the ($Cu–O_{Sr}$) bond length is remarkably shortened by intercalating mercuric bromide (13). Such a slight oxidation of the $CuO_2$ layer is surely attributed to the electron transfer from host lattice to guest layer.

The unpolarized and the polarized Bi $L_{III}$-edge XANES spectra for the pristine Bi2212 and its $HgBr_2$ intercalate are displayed in Fig. 5, in comparison with the unpolarized spectrum of Bi metal taken from Ref. (23). Three broad peaks, indicated as A, B (B′/B″) and C (C′/C″), are commonly observed for all the Bi-based cuprates. Among them, the pre-edge peak A is assigned to the $2p_{3/2} \rightarrow 6s$ transition on the basis of a previous XANES study on the $PbO_2$ (23, 24). In addition, the main-edge peaks B (B′/B″) and C (C′/C″) in the high energy side are attributed to the transitions to the $6d_{t_{2g}}$ and $6d_{e_g}$ final states, respectively (25). On the basis of their polarization dependence, the features B′ and C′ in the **E**//$c$ spectra are attributed to $2p_{3/2} \rightarrow 6d_{t_{2g}}$ ($d_{xz}$ and $d_{yz}$) and $2p_{3/2} \rightarrow 6d_{e_g}$ ($d_z^2$) transitions, while the peaks B″ and C″ in the **E**⊥$c$ spectra are assigned as $2p_{3/2} \rightarrow 6d_{t_{2g}}$ ($d_{xy}$) and $2p_{3/2} \rightarrow 6d_{e_g}$ ($d_{x-y}^2$), respectively (11). A closer comparison between both polarized spectra of the pristine Bi2212 reveals that the features B′ and C′ have higher energies with respect to the peaks B″ and C″ corresponding to the in-plane transitions, respectively. This observation can be explained by taking into account the local structure of Bi where there is a much shorter ($Bi–O_{Sr}$) axial bond (~ 1.9 Å) with respect to the other bonds, resulting in the destabilization of $d_{xz}$, $d_{yz}$, and $d_z^2$ orbitals (11, 26).

On the basis of these assignments, we have examined the evolution of Bi electronic structure upon $HgBr_2$ intercalation by comparing the spectra for the pristine Bi2212 and its $HgBr_2$ intercalate. As can be seen from Fig. 5, the $HgBr_2$ intercalation leads to a slight blue shift of the edge position, as reported previously (12), which indicates the oxidation of the BiO layer caused by electron transfer from BiO layer to bromine layer. Since the electron transferred from the BiO layer occupies the empty Br 4$p$ orbital, the charge transfer

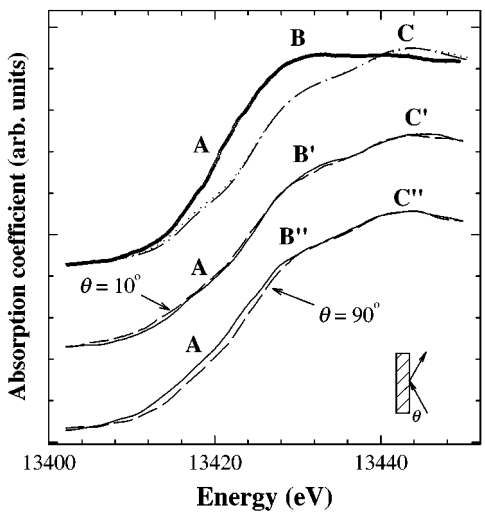


**FIG. 5.** Polarized Bi $L_{III}$-edge XANES spectra for the pristine Bi2212 single crystal (solid lines) and its $HgBr_2$ intercalate (dashed lines) with polarization angles of 10° (**E**//$c$) and 90° (**E**⊥$c$), in comparison with unpolarized spectra for Bi2212 (dotted lines), $HgBr_2$ intercalate (dot-dashed lines), and Bi metal (empty circles). For the clear depiction of spectral features, the unpolarized spectra are shifted upward along the $y$-axis.

between host and guest also contributes partially to the decrease of hole density in Br 4*p* orbital, resulting in the depression of peak A in Br K-edge XANES spectra (Fig. 3). In the viewpoint of electronic structure, such an electron transfer between the BiO layer and the $HgBr_2$ layer implies a significant orbital overlap between Bi 6*s* and Br 4*p*. In the case of polarized spectra, the shift of the edge position is dependent on polarization geometry. Namely, the main edge position in the $\mathbf{E}\perp c$ spectrum is shifted by 0.6 eV toward the high-energy side upon intercalation, confirming the oxidation of the BiO layer, whereas there is no prominent shift of edge position in the $\mathbf{E}//c$ spectrum. Besides the edge shift, the intercalation also gives rise to significant decreases in the energies of peaks B′ and C′, implying the stabilization of $6d_{t_{2g}}$ ($d_{xz}$ and $d_{yz}$) and $6d_{e_g}$ ($d_z^2$) orbitals due to a weakening of crystal field around Bi. Such a change in Bi crystal field along the *c*-axis is well consistent with the oxidation of $CuO_2$ layer, which results in a decrease of ($Cu–O_{Sr}$) bond distance and, in turn, an elongation of a competing ($Bi–O_{Sr}$) one (13). Especially, a lower shift of the peak B′ allows us to explain the anisotropic edge shift upon intercalation. That is, a downward shift of broad peak B′ might compensate the overall edge shift toward high-energy side due to the oxidation of the BiO layer, leading to a negligible change in edge position for the $\mathbf{E}//c$ spectrum.

Summarizing the present experimental findings, it becomes certain that there is a remarkable electron transfer between bromine and bismuth, implying an orbital overlap between Br 4*p* and Bi 6*s*. On the other hand, it is also found that the $HgBr_2$ intercalation increases the ionic character of the (Hg–Br) bond, that is, the electron in the semiconductive $HgBr_2$ layer becomes more localized. In this respect, the semiconducting *c*-axis resistivity of $HgBr_2$ intercalate can be attributed to the poor electrical conductivity of the intercalated mercuric bromide layer due to the enhanced electron localization in the (Hg–Br) bond.

## CONCLUSION

In this work, we have investigated the evolution of electronic structure upon $HgBr_2$ intercalation by performing polarized XAS analyses for the single crystalline Bi2212 and its $HgBr_2$ intercalate. From the present experimental findings, it becomes clear that the $HgBr_2$ intercalation gives rise not only to a significant electron transfer between bismuth and bromine but also to the electron localization in the (Hg–Br) bond, resulting in poor electronic conduction along the intercalant layer. In this context, the semiconductive *c*-axis resistivity of $HgBr_2$ intercalated Bi2212 can be explained as a result of the poor conductivity of the intercalant mercuric bromide layer, even though the orbital overlap between Bi and Br facilitates the electron conduction between host and guest along the *c*-axis.

## ACKNOWLEDGMENTS

This work was supported in part by the Korean Ministry of Science and Technology through the 1999 National Research Laboratory (NRL) project and in part by the Korean Ministry of Education through the Brain Korea 21 program. The authors are also grateful to Prof. M. Nomura for helping us to get the XAS data in the Photon Factory.

## REFERENCES

1. P. W. Anderson, *Science* **279,** 1196 (1998).
2. L. B. Ioffe and A. J. Millis, *Science* **285,** 1241 (1999).
3. T. Motohashi, Y. Nakayama, T. Fujita, K. Kitazawa, J. Shimoyama, and K. Kishio, *Phys. Rev. B* **59,** 14080 (1999).
4. G. Briceno, M. F. Crommie, and A. Zettl, *Phys. Rev. Lett.* **66,** 2164 (1991).
5. K. E. Gray and D. H. Kim, *Phys. Rev. Lett.* **70,** 1693 (1993).
6. P. W. Anderson and Z. Zou, *Phys. Rev. Lett.* **60,** 132 (1988).
7. M. F. Laguna, D. Dominguez, and C. A. Balseiro, *Phys. Rev. B* **62,** 6692 (2000).
8. X. D. Xiang, W. A. Wareka, A. Zettl, J. L. Corkill, M. L. Cohen, N. Kijima, and R. Gronsky, *Phys. Rev. Lett.* **68,** 530 (1992).
9. A. Fujiwara, Y. Koike, T. Noji, Y. Sato, T. Nishizaki, N. Kobayashi, A. Yamanaka, and F. Minami, *Phys. Rev. B* **52,** 15598 (1995).
10. J. H. Choy, S. J. Hwang, S. H. Hwang, W. Lee, D. Jung, M. Lee, and H. J. Lee, *J. Phys. Chem. B*, in press.
11. G. Liang, A. Sahiner, M. Croft, W. Xu, X. D. Xiang, D. Badresingh, W. Li, J. Chen, J. Peng, A. Zettl, and F. Lu, *Phys. Rev. B* **47,** 1029 (1993).
12. J. H. Choy, N. G. Park, S. J. Hwang, D. H. Kim, and N. H. Hur, *J. Am. Chem. Soc.* **116,** 11564 (1994).
13. J. H. Choy, S. J. Hwang, and N. G. Park, *J. Am. Chem. Soc.* **119,** 1624 (1997).
14. A. Yurgens, D. Winkler, T. Claeson, S. J. Hwang, and J. H. Choy, *Int. J. Mod. Phys. B* **13,** 3758 (1999).
15. The observed and calculated (in parentheses) weight percents of each element in $HgBr_2$ intercalated Bi2212: Hg, 10.44 (9.60); Br, 7.69 (7.65); Bi, 39.59 (40.00); Sr, 10.77 (12.58); Ca, 5.41 (5.75); Cu, 12.16 (12.16); O, 13.94 (12.26).
16. H. Oyanagi, T. Matsushida, M. Ito, and H. Kuroda, *KEK Report* **83,** 30 (1984); H. Kuroda and A. Koyama, *KEK Report* **84,** 19 (1989).
17. R. Åkesson, I. Persson, M. Sandstrom, and U. Wahlgren, *Inorg. Chem.* **33,** 3715 (1994).
18. In order to probe the detailed variation of peak intensity upon $HgBr_2$ intercalation, the unpolarized spectrum of reference $HgBr_2$ is compared with that of polycrystalline $HgBr_2$ intercalate, rather than the corresponding polarized spectra.
19. According to the previous EXAFS analyses at Hg $L_{III}$-edge (Ref. 13), it is evident that the intercalated $HgBr_2$ is stabilized as a linear molecule with two coordination number of mercury. On the other hand, the mercury ion in the reference $HgBr_2$ solid is coordinated with two neighboring bromide ions ($d_{Hg-Br} = 2.46$ Å) as well as with four remote bromide ions ($d_{Hg-Br} = 3.23$ Å). Actually, this compound is regarded as a kind of molecular solid with linear $HgBr_2$ moiety due to the severe distortion of $HgBr_6$ octahedron. In this regard, it can be expected that the variation of coordination number upon intercalation has little influence on the hole density of mercury in $HgBr_2$, and hence the observed enhancement of peak A is surely attributable to the increase of ionicity of the (Hg–Br) bond rather than the variation of coordination number.
20. J. H. Choy, S. J. Hwang, and D. K. Kim, *Phys. Rev. B* **55,** 5674 (1997).

21. Considering the tilting angle of $HgBr_2$ linear molecule with respect to the $c$-axis (65°), the Br K-edge XANES spectrum with $\mathbf{E}//c$ geometry reflects mainly the transition from the $1s$ orbital to the $4p_\pi^*$ one, whereas the $1s \rightarrow 4p_\sigma^*$ transition contributes to the spectral features in the $\mathbf{E} \perp c$ spectrum.
22. J. H. Choy, D. K. Kim, S. H. Hwang, and G. Demazeau, *Phys. Rev. B* **50,** 16631 (1994).
23. R. Retoux, F. Studer, C. Michel, B. Raveau, A. Fontaine, and E. Dartyge, *Phys. Rev. B* **41,** 193 (1990).
24. K. J. Rao and J. Wong, *J. Chem. Phys.* **81,** 4832 (1984).
25. F. Studer, D. Bourgault, C. Martin, R. Retoux, C. Michael, B. Raveau, E. Dartyge, and A. Fontaine, *Physica C* **159,** 609 (1989).
26. A. Bianconi, C. Li, F. Campanella, S. D. Longa, I. Pettiti, M. Pompa, S. Turtu, and D. Udron, *Phys. Rev. B* **44,** 4560 (1991).